Resource Distribution Under Spatiotemporal Uncertainty of Disease Spread: Stochastic versus Robust Approaches

Beste Basciftci[*] Xian Yu[†] Siqian Shen[‡]

Abstract

Speeding up testing and vaccination is essential to controlling the coronavirus disease 2019 (COVID-19) pandemic that has become a global health crisis. In this paper, we develop mathematical frameworks for optimizing locations of distribution centers and plans for distributing resources such as test kits and vaccines under spatiotemporal uncertainties of disease infections and demand for the resources. The goal is to balance between operational cost (including costs of deploying facilities, shipping, and storage) and quality of service (reflected by delivery speed and demand coverage), while ensuring equity and fairness of resource distribution across multiple populations. We compare solutions of a stochastic integer program with robust solutions under the distributional ambiguity of demand. For the latter, we propose a distributionally robust optimization model using a moment ambiguity set. We conduct numerical studies by solving instances of distributing COVID vaccines in the United States and test kits in the State of Michigan and compare our solutions with the ones implemented in real world. We demonstrate results over distinct phases of the pandemic to estimate cost and speed of resource distribution depending on the scales and coverage.

Keywords: COVID-19 pandemic; vaccine distribution; resource allocation; stochastic integer programming; distributionally robust optimization; multi-objective optimization

1 Introduction

With the rapid spread of the coronavirus disease 2019 (COVID-19), testing is central to planning response activities in all countries during and post the pandemic. Effective and efficient testing can lead to early outbreak detection, to quickly isolate and treat infected patients, guide people consciously performing social distancing, and also lock down certain areas/activities if needed. Hence, to keep the pandemic under control or prepare for the next wave, well-planned, strategic testing is necessary for both disease prevention and intervention (CDC, 2020). Establishing such a

---

[*]Industrial Engineering Program, Sabanci University, Istanbul, Turkey, Email: beste.basciftci@sabanciuniv.edu;

[†]Department of Industrial and Operations Engineering, University of Michigan at Ann Arbor, Email: yuxian@umich.edu;

[‡]Corresponding author; Department of Industrial and Operations Engineering, University of Michigan at Ann Arbor, Email: siqian@umich.edu.

system involves distributing test kits to test centers while considering potential demand uncertainty for testing (see, e.g., Lampariello and Sagratella, 2021; Santini, 2021). Such a resource distribution problem also arises in the production and distribution of COVID-19 vaccines that recently became available – That is, upon needs and orders from different regions, a central government sends limited amounts of vaccines to local agents using the information of regional infection status. This problem was solved in the United States (US) during the first four months of Year 2021 for distributing the COVID vaccines and is widely applicable when vaccines become available globally, or for distributing resources to respond to future outbreaks of other diseases.

The literature in vaccine operations mainly consider designing vaccine allocation policies targeting on specific population groups or regions (Westerink-Duijzer, 2017) for responding to outbreaks of various types of diseases including influenza and Ebola (see, e.g., Medlock and Galvani, 2009; Long et al., 2018; Li et al., 2018). For COVID-19 specifically, Bubar et al. (2020) discuss strategies for vaccine prioritization among different population groups; Babus et al. (2020) estimate occupation-based infection risks and use age-based infection fatality rates in a model to assign priorities over populations with different occupations and ages; Bertsimas et al. (2020) capture vaccine effects and the variability in mortality rates across sub-populations, and then integrate a predictive model into a prescriptive model to optimize vaccine allocation; Chen et al. (2020) focus on how priority and population groups should be identified over time under limited supply.

In the US, with the Biden Administration pledging "100 million vaccine shorts in 100 days," policymakers seek the most efficient way to distribute vaccines to states and jurisdictions, and then to local hospitals, clinics, pharmacies, schools, communities and so on. Given certain vaccine allocation policies, how to distribute vaccines from production sites or DCs to downstream demand is challenging and emergent. However, it is hard to quantify the cost and speed trade-off for distributing vaccines or test kits, as there exist hidden costs associated with unsatisfied demand that may come from high-risk groups. It is also challenging to locate DCs and make shipping plans optimally to achieve the best trade-off, given the evolving pandemic and rapidly changing demand. Moreover, the scale of the problem can be enormous, involving millions of vaccines (or test kits) and large-scale distributed demand for operating the system for the whole country. A scientific way to conduct vaccine and test kit distribution needs to rely on mathematical models and algorithms for processing and utilizing information from large datasets about the COVID-19 infection trends and demand for testing/vaccination.

Duijzer et al. (2018) present a comprehensive review of the literature on vaccine supply chain management, covering both methodologies and applications. Golan et al. (2020) conduct a review of the literature that focuses on the resilience of vaccine supply chains, and point out that the lack of network-based, modeling-based, quantitative analysis is a major gap in the literature that needs to be bridged in order to create methods of real-time analysis and decision tools for the COVID-19 vaccine supply chain. Indeed, as the majority of the literature focusing on COVID-19 vaccine allocation, few studies develop mathematical approaches for solving the operational problems related to vaccine distribution. Among them, Bertsimas et al. (2021b) optimize vaccine site selection and the assignment of population to different sites while ensuring optimal subsequent

vaccine allocation. They show that the proposed solution achieves critical fairness objectives and is also highly robust to uncertainties and forecasting errors. Other types of vaccine-related operational problems involve locating facilities to produce or store vaccines and shipping them to demand in a daily basis, which are investigated in this paper.

There has been a large body of research studies on how to site retail stores, optimize inventory and production, manage stock levels as demand for products fluctuates by season (Daskin, 2011; Shen et al., 2011; Snyder, 2006; Basciftci et al., 2020). Among them, many focus on the resilience and reliability of facility locations under uncertain demand and disruptions, using stochastic or robust optimization approaches. Establishing an operational system for COVID-19 resource distribution presents a very similar set of challenges but under disease spread and demand uncertainties.

In this study, we present a mathematical framework that encapsulates allocation and distribution stages of disease-control resources (e.g., vaccines and test kits) by considering spatiotemporal uncertainty in their demand and ambiguity of the demand distribution over a multi-period planning horizon. We optimize the locations of resource DCs, their capacities, shipment amounts and inventory levels. As the provided framework is presented in a generic form, it aims to address various resource allocation problems during different phases of a pandemic by comparing deterministic, stochastic and distributionally robust decision-making approaches for different scenarios in practice.

The main contributions of the paper are threefold. First, we combine mathematical programming and statistical learning, for optimally locating DCs for disease-control resources and deriving shipping plans, customized for counties and states with diverse demographics and disease spread patterns. Our research can be utilized at the national level to balance the distribution, or at the state or county level to facilitate local operations. Second, through data-informed location optimization, we can effectively identify the most critical and vulnerable groups to prioritize testing or receiving vaccines under constrained amounts of resources and as a result, can protect other population groups. Third, we conduct extensive numerical studies using real COVID-19 infection data in the US and in the State of Michigan, to compare different approaches under demand uncertainty. We compare the operational cost and speed of resource distribution based on a diverse set of instances having different scales and parameter settings.

The rest of the paper is organized as follows. In Section 2, we review the most relevant literature in disease control, and its related facility location and supply chain management. In Section 3, we present the stochastic optimization model based on a set of demand samples generated from a given probability distribution and in Section 4, we consider that the exact demand distribution is unknown and optimize decisions against the distributional ambiguity. In Section 5, we conduct numerical studies using COVID-19 infection data to demonstrate results of distributing vaccines and test kits, and compare our solutions with what were implemented by the Center of Disease Control (CDC) in the US. In Section 6, we conclude the paper and present future research directions.

2   Literature Review

Resource distribution is of vital importance in many applications, in particular the ones related to disease control and disaster relief, as the resources are usually scarce (Cao and Huang, 2012). In post disaster relief, the time efficiency for distributing resources is an important concern (Gupta et al., 2016), e.g., in ambulances dispatch (see, e.g., Gong and Batta, 2007) and allocating medical resources to patients with deteriorating health conditions (see, e.g., Xiang and Zhuang, 2016). For COVID-19, personal protective equipment (PPE), test kits, hospital beds and ventilators, and, most recently, vaccines are among the resources that need to be effectively distributed at all levels (see, Emanuel et al., 2020). For example, Bertsimas et al. (2021a) formulate a deterministic optimization model to improve ventilator allocation by allowing sharing of ventilators between hospitals from different states. Billingham et al. (2020) study a similar problem to optimize ventilator sharing. Furthermore, hospital bed allocation has been considered by Zachary A. Collier et al. (2020) through identifying "hot spot" regions that have spikes in the number of infected cases and using a value-based optimization model that measures the value based on the usage of marginal medical resources. However, the above studies predict the number of patients in critical conditions using forecasting, and the inherent uncertainty is not explicitly considered within planning. Mehrotra et al. (2020); Blanco et al. (2020) propose stochastic programming approaches to address this issue by generating scenarios with different patterns to represent patient amount uncertainty, to re-allocate and share medical resources among different hospitals. Recently, Parker et al. (2020) use robust optimization by assuming an unknown number of patients for each specific day within a certain range from a nominal value, e.g., the average across a certain period.

Lampariello and Sagratella (2021) consider a single-period COVID test kit allocation problem by maximizing utility functions corresponding to disease detection capabilities in different regions while determining the amount of test kits to be allocated in each region given a certain budget. Santini (2021) considers the distribution of swabs and reagent to laboratories for maximizing the number of COVID tests processed. The author formulates the problem as a deterministic integer programming model by considering sharing of swabs and reagent among different laboratories over a multi-period planing horizon. Although the above studies focus on different stages of the testing-related resource planning problems, the infection uncertainty in different regions and periods, is not incorporated to obtain reliable solutions over expected or worst-case performances. Moreover, the probability distribution of the uncertain demand for resources may be ambiguous during emergency or disaster relief operations due to the inherent and abrupt nature of these events (see, e.g., Liu et al., 2019; Wang and Chen, 2020). This motivates the development of a distributionally robust optimization approach in our paper for robustly allocating resources in an unprecedented event setting such as the COVID-19 pandemic.

The supply chain operations of vaccines for infectious disease control involve production, allocation and distribution stages, with decisions on which vaccines to produce, how many doses to produce, who should be vaccinated, how the vaccines can be distributed, and so on (see Duijzer et al., 2018). Özaltın et al. (2011) present a multi-stage stochastic programming approach to

determine vaccine composition and timing of these decisions in preparation for annual influenza. The production phase takes into account objectives from both vaccine manufacturers and government agencies while considering uncertainties in both sides of supply and demand (Chick et al., 2008). Equitable and timely allocation of vaccines to different population groups becomes necessary in order to eliminate infectious diseases worldwide (Tebbens and Thompson, 2009). In that regard, Huang et al. (2017) provide a retrospective study over 2009 H1N1 pandemic by developing deterministic optimization models to ensure fair and equitable allocation of vaccines through first determining coverage levels of each region and then finding an allocation plan within certain tolerance from the targeted levels. In addition to the vaccine-allocation studies, Jacobson et al. (2006) point out that vaccine doses need to be distributed to end-users through determining which locations these resources should be kept and how many units should be stored as inventory.

3 A Stochastic Optimization Approach

In this paper, we consider the distribution of vaccines or test kits in a given region as a capacitated facility location problem involving multiple periods of shipment planning. A decision maker may need to solve the problem for either national- or state-level operations, to distribute manufactured vaccines and test kits to different states or counties from located DCs. Here, the DCs could also be the manufacturing sites, as manufactures can dispatch productions to states or to counties directly, given their demand. In addition, the federal or state governments can act to open up new DCs to improve the efficiency of operations and increase demand coverage.

We denote $\mathcal{I}$, $\mathcal{J}$, $\mathcal{T}$ as the sets of potential sites for locating DCs, demand locations and finite periods, respectively. Let c_i^o, c_i^h, c_{ijt}^s, c_{jt}^u, c_{jt}^I be the cost of operating DC i, unit cost of installing capacities in DC i, unit shipping cost from DC i to demand site j in period t, unit penalty cost of unsatisfied demand and unit cost of inventory at demand site j in period t, for all $i \in \mathcal{I}$, $j \in \mathcal{J}$, $t \in \mathcal{T}$, respectively. (Varying cost parameter c_{jt}^u can help ensure fair resource distribution to prioritized demand locations based on their demographics and infection status over time.) We denote B_t as the total capacity of manufacturing resources across all DCs in period t for all $t \in \mathcal{T}$, determined by the total amount of raw materials, space, workers, etc., needed for manufacturing the resources during each period. Let $\boldsymbol{d}$ denote the vector of uncertain demand (i.e., the number of people who need to be vaccinated or tested) and let P be its probability distribution. We use the Monte Carlo sampling approach (Kleywegt et al., 2002) to replace P with an empirical distribution constructed by $|\Omega|$ scenarios with each scenario $\omega \in \Omega$ having an equal probability $p^\omega = 1/|\Omega|$. In this regard, we consider a finite set Ω of realizations of the random vector $\boldsymbol{d}$. Specifically, for each scenario $\omega \in \Omega$, we use $d_{jt}(\omega)$ to represent the demand realization at site j in period t for all $j \in \mathcal{J}$ and $t \in \mathcal{T}$, and therefore $\boldsymbol{d} = [d_{jt}(\omega), \ \omega \in \Omega, \ j \in \mathcal{J}, \ t \in \mathcal{T}]^\mathsf{T}$. For notation convenience, bold letters are used for representing vectors and matrices throughout this paper.

Define binary variables $x_i \in \{0, 1\}$, $\forall i \in \mathcal{I}$ such that $x_i = 1$ if DC i is built, and $x_i = 0$ otherwise. For each built DC i and period $t \in \mathcal{T}$, we also decide its capacity $h_{it} \geq 0$ for manufacturing or storing the resources. Both variables $\boldsymbol{x}$ and $\boldsymbol{h}$ are planning decisions and their values need to be

determined before realizing uncertain demand $\boldsymbol{d}$. For each scenario $\omega \in \Omega$, we define variables $s_{ijt}(\omega) \geq 0$ to be the amounts of resources sent from DC i to demand location j in period t, for all $i \in \mathcal{I}$, $j \in \mathcal{J}$, $t \in \mathcal{T}$. For each demand site $j \in \mathcal{J}$, we allow to keep inventory if the received resources are more than the total demand or to back order otherwise. In particular, we assume that people who cannot receive vaccines or test kits in the current period will wait to be administered in future periods. Accordingly, we define variables $I_{jt}(\omega) \geq 0$ and $u_{jt}(\omega) \geq 0$ as the inventory and backlog recourse variables for each $j \in \mathcal{J}$, $t \in \mathcal{T}$, and $\omega \in \Omega$. Moreover, input parameters I_{j0} and u_{j0} denote the initial inventory and backlog at demand location j for all $j \in \mathcal{J}$, whose values are the same across all scenarios.

We first employ a two-stage stochastic mixed-integer linear programming (TS-MILP) framework to formulate the problem, where in the first stage, we decide values of variables x_i and h_{it} for all $i \in \mathcal{I}$, $t \in \mathcal{T}$. In the second stage, given each demand value $d_{jt}(\omega)$, we optimize the corresponding shipping and inventory plans using variables $s_{ijt}(\omega)$, $I_{jt}(\omega)$ and $u_{jt}(\omega)$ for each scenario $\omega \in \Omega$.

The TS-MILP model is given by:

$$\min \quad \sum_{i\in\mathcal{I}} c_i^o x_i + \sum_{i\in\mathcal{I},t\in\mathcal{T}} c_i^h h_{it} + \sum_{\omega\in\Omega} p^\omega \left(\sum_{i\in\mathcal{I},j\in\mathcal{J},t\in\mathcal{T}} c_{ijt}^s s_{ijt}(\omega) + \sum_{j\in\mathcal{J},t\in\mathcal{T}} \left(c_{jt}^I I_{jt}(\omega) + c_{jt}^u u_{jt}(\omega) \right) \right) \quad (1a)$$

$$\text{s.t.} \quad h_{it} \leq M_i x_i, \ \forall i \in \mathcal{I}, \ t \in \mathcal{T}, \quad (1b)$$

$$\sum_{i\in\mathcal{I}} h_{it} \leq B_t, \ \forall t \in \mathcal{T}, \quad (1c)$$

$$\sum_{j\in\mathcal{J}} s_{ijt}(\omega) \leq h_{it}, \ \forall i \in \mathcal{I}, \ t \in \mathcal{T}, \ \omega \in \Omega, \quad (1d)$$

$$\sum_{i\in\mathcal{I}} s_{ijt}(\omega) + I_{jt-1}(\omega) + u_{jt}(\omega) = d_{jt}(\omega) + I_{jt}(\omega) + u_{jt-1}(\omega), \ \forall j \in \mathcal{J}, \ t \in \mathcal{T}, \ \omega \in \Omega, \quad (1e)$$

$$x_i \in \{0,1\}, \ h_{it}, \ s_{ijt}(\omega), \ I_{jt}(\omega), \ u_{jt}(\omega) \geq 0, \ \forall i \in \mathcal{I}, \ j \in \mathcal{J}, \ t \in \mathcal{T}, \ \omega \in \Omega, \quad (1f)$$

where the objective function (1a) minimizes the total cost of opening DCs, installing their capacities, and the total expected cost of shipping, holding inventory and back-orders. Constraints (1b) prohibit assigning any capacity to a DC that is not in use, where M_i is the capacity limit of the DC i for all $i \in \mathcal{I}$. Constraints (1c) impose temporal limitation on the total amount of production capacities for all DCs. Constraints (1d) link the first-stage variables with the second-stage recourse decisions such that the total shipment from each DC is no more than its installed capacity during any period in any scenario. Constraints (1e) are "flow-balance" constraints to reflect the changes of inventory and back-order levels, depending on the amount of resources received and demand level at each site j, for each period t in each scenario ω. Constraints (1f) require binary valued x-variables and set all the other variables to be non-negative.

Constraints (1d) contain bilinear terms $h_i x_i$ for all $i \in \mathcal{I}$, which can be reformulated linearly using McCormick envelopes, as variables x_i, $\forall i \in \mathcal{I}$ are binary-valued. Specifically, we let $\bar{h}_i$ be the upper bounds on variables h_i for all $i \in \mathcal{I}$, and replace Constraints (1d) with the following

constraints.

$$\sum_{j \in \mathcal{J}} s_{ijt}(\omega) \le z_i, \ \forall i \in \mathcal{I}, \ t \in \mathcal{T}, \ \omega \in \Omega$$

$$0 \le z_i \le \bar{h}_i x_i, \ \forall i \in \mathcal{I},$$

$$h_i - (1 - x_i)\bar{h}_i \le z_i \le h_i, \ \forall i \in \mathcal{I}.$$

3.1   Model extension I: Inventory at DCs

When the costs of production capacity (c_{it}^h) and shipment (c_{ijt}^s) are time-independent, it is without loss of generality to assume that there is no inventory kept in DCs because those additional products can be shipped to and stored at customer sites. However, if these costs vary over time, it may be beneficial to keep some products in DCs and ship them in the future. In this case, we define additional variables $I_{i,t}^D(\omega)$ as the inventory at DC i in period t with scenario ω for all $i \in \mathcal{I}$, $t \in \mathcal{T}$, $\omega \in \Omega$. Accordingly, Constraints (1d) can be modified as follows:

$$\sum_{j \in \mathcal{J}} s_{ijt}(\omega) + I_{i,t}^D(\omega) = h_{it} + I_{i,t-1}^D(\omega), \ \forall i \in \mathcal{I}, \ t \in \mathcal{T}, \ \omega \in \Omega,$$

where $I_{i,0}^D(\omega) = I_{i,0}^D, \ \forall \omega \in \Omega$ is the (given) initial inventory at DC i. Moreover, the objective function (1a) can be recast as

$$\sum_{i \in \mathcal{I}} c_i^o x_i + \sum_{i \in \mathcal{I}, t \in \mathcal{T}} c_{it}^h h_{it} + \sum_{\omega \in \Omega} p^\omega \left(\sum_{i \in \mathcal{I}, j \in \mathcal{J}, t \in \mathcal{T}} c_{ijt}^s s_{ijt}(\omega) + \sum_{i \in \mathcal{I}, t \in \mathcal{T}} c_{it}^{ID} I_{i,t}^D(\omega) + \sum_{j \in \mathcal{J}, t \in \mathcal{T}} \left(c_{jt}^I I_{j,t}(\omega) + c_{jt}^u u_{jt}(\omega) \right) \right)$$

where c_{it}^{ID} is the unit inventory cost at DC i in period t for all $i \in \mathcal{I}$, $t \in \mathcal{T}$.

Remark 1. Model (1) assumes that there is no lead time when shipping from DCs to demand locations. In the case of a constant lead time for every DC and demand-location pairs, we can simply shift the optimal production and shipment plans accordingly. However, if the lead time varies by location, it is worthwhile to add lead time into our model. We denote L_{ij} as the lead time in sending resources from DC i to customer location j for all $i \in \mathcal{I}$, $j \in \mathcal{J}$. Then, Constraints (1e) can be adjusted to

$$\sum_{i \in \mathcal{I}: t \ge L_{ij}} s_{ijt-L_{ij}}(\omega) + I_{jt-1}(\omega) + u_{jt}(\omega) = d_{jt}(\omega) + I_{jt}(\omega) + u_{jt-1}(\omega), \ \forall j \in \mathcal{J}, \ t \in \mathcal{T}, \ \omega \in \Omega. \quad (2)$$

4   A Distributionally Robust Approach

The two-stage stochastic programming approach introduced in Section 3 assumes that the distribution of the underlying uncertainty is perfectly known and one can have access to a large amount of samples from the true distribution. However, these may not be true in practice, specifically during a pandemic, where the distribution may be misspecified under limited information. To model this type of distributional ambiguity, we consider a distributionally robust optimization model, in which

optimal solutions are sought for the worst-case probability distribution within a family of candidate distributions, called an "ambiguity set" and denoted by $\mathcal{P}$. We denote the random demand vector by $\boldsymbol{\xi} = [d_{jt}, \ j \in \mathcal{J}, \ t \in \mathcal{T}]^{\top}$ and the unknown probability distribution by $\mathbb{P}$. A distributionally robust analogous model of the two-stage stochastic program (1) is:

$$\min \quad \sum_{i \in \mathcal{I}} c_i^o x_i + \sum_{i \in \mathcal{I}, t \in \mathcal{T}} c_i^h h_{it} + \max_{\mathbb{P} \in \mathcal{P}} \mathbb{E}[g(\boldsymbol{h}, \boldsymbol{\xi})] \tag{3a}$$

$$\text{s.t.} \quad h_{it} \leq M_i x_i, \ \forall i \in \mathcal{I}, \ t \in \mathcal{T}, \tag{3b}$$

$$\sum_{i \in \mathcal{I}} h_{it} \leq B_t, \ \forall t \in \mathcal{T}, \tag{3c}$$

$$x_i \in \{0,1\}, \ h_{it} \geq 0, \ \forall i \in \mathcal{I}, \ t \in \mathcal{T}, \tag{3d}$$

where

$$g(\boldsymbol{h}, \boldsymbol{\xi}) = \min \quad \sum_{i \in \mathcal{I}, j \in \mathcal{J}, t \in \mathcal{T}} c_{ijt}^s s_{ijt} + \sum_{j \in \mathcal{J}, t \in \mathcal{T}} \left(c_{jt}^I I_{jt} + c_{jt}^u u_{jt} \right) \tag{4a}$$

$$\text{s.t.} \quad \sum_{j \in \mathcal{J}} s_{ijt} \leq h_{it}, \ \forall i \in \mathcal{I}, \ t \in \mathcal{T}, \tag{4b}$$

$$\sum_{i \in \mathcal{I}} s_{ijt} + I_{jt-1} + u_{jt} = \xi_{jt} + I_{jt} + u_{jt-1}, \ \forall j \in \mathcal{J}, \ t \in \mathcal{T}, \tag{4c}$$

$$s_{ijt}, \ I_{j,t}, \ u_{jt} \geq 0, \ \forall i \in \mathcal{I}, \ j \in \mathcal{J}, \ t \in \mathcal{T}. \tag{4d}$$

The objective function (3a) minimizes the cost of opening DCs, installing their capacities, and the worst-case expected cost under the set of candidate distributions in the ambiguity set $\mathcal{P}$. The inner problem (4) corresponds to the second-stage problem and minimizes the total cost of shipping, holding inventory and backlogging given first-stage decision $\boldsymbol{h}$.

To express the form of uncertainty in distribution, two main classes of ambiguity sets can be defined for distributionally robust optimization models. They are (i) statistical distance-based ambiguity sets that consider distributions within a certain distance to a reference distribution (Jiang and Guan, 2016; Mohajerin Esfahani and Kuhn, 2018), and (ii) moment-based ambiguity sets that consider distributions based on moment information (Delage and Ye, 2010; Zhang et al., 2018). Since a reference distribution is essential in constructing the former class of ambiguity sets, such a distribution might be misleading in the case of a pandemic with abrupt and unprecedented changes in events and requires further data points to ensure its accuracy with a high level of confidence. Therefore, we focus on the moment-based ambiguity sets for describing possible distributions corresponding to the underlying demand uncertainty.

To construct our ambiguity set, we bound a set of moment functions of $\boldsymbol{\xi}$ by certain parameters. Specifically, we consider m different moment functions $\boldsymbol{f} := (f_1(\boldsymbol{\xi}), \ldots, f_m(\boldsymbol{\xi}))^{\top}$. Assuming that the random vector $\boldsymbol{\xi}$ has a finite support set S containing possible realizations $S = \{\boldsymbol{\xi}^1, \cdots, \boldsymbol{\xi}^K\}$, for a given distribution $\mathbb{P}$, we reformulate $\mathbb{E}[g(\boldsymbol{h}, \boldsymbol{\xi})]$ as $\sum_{k \in [K]} p_k g(\boldsymbol{h}, \boldsymbol{\xi}^k)$. Consequently, the inner problem (4) can be represented for each realization from the set $\{\boldsymbol{\xi}^1, \cdots, \boldsymbol{\xi}^K\}$. Then for each $s = 1, \ldots, m$, the corresponding moment function $f_s(\boldsymbol{\xi}) = \prod_{j \in \mathcal{J}, t \in \mathcal{T}} \xi_{jt}^{k_{sjt}}$, where k_{sjt} is a non-negative integer indicating the power of ξ_{jt} for the s-th moment function. The lower and upper

bounds are defined by $\boldsymbol{l} := (l_1, \ldots, l_m)^\mathsf{T}$ and $\boldsymbol{u} := (u_1, \ldots, u_m)^\mathsf{T}$, respectively. Correspondingly, we specify the ambiguity set $\mathcal{P}$ as follows.

$$\mathcal{P} := \left\{ \boldsymbol{p} \in \mathbb{R}_+^K \mid \boldsymbol{l} \leq \sum_{k \in [K]} p_k \boldsymbol{f}(\boldsymbol{\xi}^k) \leq \boldsymbol{u} \right\}. \tag{5}$$

Note that to guarantee that the ambiguity set (5) defines a set of probability distributions, one of the moment functions of $\boldsymbol{f}$ and its corresponding lower and upper bound values l_s, u_s, can be set as $\sum_{k \in [K]} p_k = 1$. The following theorem demonstrates a reformulation of Model (3) given the moment-based ambiguity set in (5).

Theorem 1. If the ambiguity set defined in (5) is non-empty, then Model (3) can be reformulated as a monolithic problem:

$$\min \quad \sum_{i \in \mathcal{I}} c_i^o x_i + \sum_{i \in \mathcal{I}, t \in \mathcal{T}} c_i^h h_{it} - \boldsymbol{\alpha}^\mathsf{T} \boldsymbol{l} + \boldsymbol{\beta}^\mathsf{T} \boldsymbol{u} \tag{6a}$$

$$\text{s.t.} \quad \text{(3b)}–\text{(3d)}$$

$$(-\boldsymbol{\alpha} + \boldsymbol{\beta})^\mathsf{T} \boldsymbol{f}(\boldsymbol{\xi}^k) \geq g(\boldsymbol{h}, \boldsymbol{\xi}^k), \ \forall k \in [K], \tag{6b}$$

$$\boldsymbol{\alpha}, \ \boldsymbol{\beta} \geq 0. \tag{6c}$$

Proof. Explicitly stating the constraints in the ambiguity set $\mathcal{P}$, we first express the inner maximization problem as

$$\max \quad \sum_{k \in [K]} p_k g(\boldsymbol{h}, \boldsymbol{\xi}^k) \tag{7a}$$

$$\text{s.t.} \quad \sum_{k \in [K]} p_k \boldsymbol{f}(\boldsymbol{\xi}^k) \geq \boldsymbol{l}, \tag{7b}$$

$$\sum_{k \in [K]} p_k \boldsymbol{f}(\boldsymbol{\xi}^k) \leq \boldsymbol{u}, \tag{7c}$$

$$p_k \geq 0, \ \forall k \in [K]. \tag{7d}$$

Letting $\boldsymbol{\alpha}, \boldsymbol{\beta}$ be the dual variables associated with the lower- and upper-bound constraints in (7), respectively, we obtain its dual formulation as

$$\min_{\boldsymbol{\alpha}, \boldsymbol{\beta}} \quad -\boldsymbol{\alpha}^\mathsf{T} \boldsymbol{l} + \boldsymbol{\beta}^\mathsf{T} \boldsymbol{u} \tag{8a}$$

$$\text{s.t.} \quad (-\boldsymbol{\alpha} + \boldsymbol{\beta})^\mathsf{T} \boldsymbol{f}(\boldsymbol{\xi}^k) \geq g(\boldsymbol{h}, \boldsymbol{\xi}^k), \ \forall k \in [K], \tag{8b}$$

$$\boldsymbol{\alpha}, \ \boldsymbol{\beta} \geq 0. \tag{8c}$$

Following the strong duality between (7) and (8), and replacing $\max_{\boldsymbol{p} \in \mathcal{P}} \sum_{k \in [K]} p_k g(\boldsymbol{h}, \boldsymbol{\xi}^k)$ with (8) in the outer optimization problem (3), we obtain the desired result. $\qquad \square$

Next we examine a special form of ambiguity set (5), where for the first and second moments of each demand parameter, we consider their lower and upper bounds as follows:

$$\mathcal{P} = \left\{ \boldsymbol{p} \in \mathbb{R}_+^K \mid \sum_{k \in [K]} p_k = 1, \right. \tag{9a}$$

$$\mu_{jt} - \epsilon_{jt}^\mu \leq \sum_{k \in [K]} p_k \xi_{jt}^k \leq \mu_{jt} + \epsilon_{jt}^\mu, \ \forall j \in \mathcal{J}, \ t \in \mathcal{T}, \tag{9b}$$

$$\left. S_{jt} \underline{\epsilon}_{jt}^S \leq \sum_{k \in [K]} p_k (\xi_{jt}^k)^2 \leq S_{jt} \bar{\epsilon}_{jt}^S, \ \forall j \in \mathcal{J}, \ t \in \mathcal{T} \right\}. \tag{9c}$$

Here, the empirical first and second moments of the uncertain demand parameter at location j and period t are denoted by μ_{jt} and S_{jt}, respectively. Constraint (9a) is a normalization constraint to ensure that $\{p_k\}_{k \in [K]}$ form a probability distribution. Constraints (9b) bound the mean of parameter ξ_{jt} in an ϵ_{jt}^μ-interval of the empirical mean μ_{jt}, and constraints (9c) bound the second moment of parameter ξ_{jt} via scaling the empirical second moment S_{jt} with parameters $0 \leq \underline{\epsilon}_{jt}^S \leq 1 \leq \bar{\epsilon}_{jt}^S$ for all $j \in \mathcal{J}$, $t \in \mathcal{T}$. We note that under the perfect knowledge assumption of first and second moment information, the robustness parameters can be set as $\epsilon_{jt}^\mu = 0$, and $\underline{\epsilon}_{jt}^\sigma = \bar{\epsilon}_{jt}^\sigma = 1$, for all $j \in \mathcal{J}$, $t \in \mathcal{T}$. Under the uncertainty of a pandemic, adjusting these parameters helps decision makers make inferences for representing spatiotemporal demand by considering different phases of the pandemic and taking into account potential deviations from predictive results.

To obtain a mixed-integer linear programming reformulation of the monolithic formulation (6) given ambiguity set (9), we first describe some intermediate steps and results. In this regard, we analyze certain properties of the function $g(\boldsymbol{h}, \boldsymbol{\xi}^k)$.

Proposition 1. Function $g(\boldsymbol{h}, \boldsymbol{\xi}^k)$ is a convex piecewise linear function in $\boldsymbol{h}$ for every $k \in [K]$.

Proof. First, note that problem (4) is always feasible as it has complete recourse. Letting θ_{it}, γ_{jt} be the dual variables, we obtain the dual of problem (4) as follows.

$$\max \quad \sum_{i \in \mathcal{I}} \sum_{t \in \mathcal{T}} h_{it} \theta_{it} + \sum_{j \in \mathcal{J}} \sum_{t=2}^{T} \xi_{jt}^k \gamma_{jt} + \sum_{j \in \mathcal{J}} (\xi_{j1}^k + u_{j0} - I_{j0}) \gamma_{j1} \tag{10a}$$

$$\text{s.t.} \quad \theta_{it} + \gamma_{jt} \leq c_{ijt}^s, \ \forall i \in \mathcal{I}, \ j \in \mathcal{J}, \ t \in \mathcal{T}, \tag{10b}$$

$$- \gamma_{jt} + \gamma_{jt+1} \leq c_{jt}^I, \ \forall j \in \mathcal{J}, \ t \in \{1, \cdots, T-1\}, \tag{10c}$$

$$- \gamma_{jT} \leq c_{jT}^I \ \forall j \in \mathcal{J}, \tag{10d}$$

$$\gamma_{jt} - \gamma_{jt+1} \leq c_{jt}^u, \ \forall j \in \mathcal{J}, \ t \in \{1, \cdots, T-1\}, \tag{10e}$$

$$\gamma_{jT} \leq c_{jT}^u \ \forall j \in \mathcal{J}, \tag{10f}$$

$$\theta_{it} \leq 0 \ \forall i \in \mathcal{I}, \ t \in \mathcal{T}. \tag{10g}$$

As the dual problem (10) is feasible, at least one of the optimal solutions of this problem is at one of its extreme points. Considering the fact that objective function of this problem is linear in $\boldsymbol{h}$, the

resulting optimal objective value can be represented as the maximum of the extreme-point-based function values. Hence, $g(\boldsymbol{h}, \boldsymbol{\xi}^k)$ becomes a convex piecewise linear function in $\boldsymbol{h}$. $\square$

Lemma 1. Denote $g(\boldsymbol{h}, \boldsymbol{\xi}^k)$ by a compact form $\min_{\boldsymbol{y}}\{\boldsymbol{c}^\top \boldsymbol{y} : \boldsymbol{A}\boldsymbol{y} \geq \boldsymbol{h}, \boldsymbol{D}\boldsymbol{y} \geq \boldsymbol{f}\}$. Then, set $\Upsilon^1 := \{(\boldsymbol{h}, m) : g(\boldsymbol{h}, \boldsymbol{\xi}^k) \leq m\}$ for each $\boldsymbol{\xi}^k \in S$ has a polyhedral representation $\Upsilon^2 := \{(\boldsymbol{h}, m) : \exists \boldsymbol{y} \text{ s.t. } \boldsymbol{c}^\top \boldsymbol{y} \leq m, \ \boldsymbol{A}\boldsymbol{y} \geq \boldsymbol{h}, \ \boldsymbol{D}\boldsymbol{y} \geq \boldsymbol{f}\}$.

Proof. Demonstrated in Proposition 1, $g(\boldsymbol{h}, \boldsymbol{\xi}^k)$ is a convex function. Consider any $(\boldsymbol{h}, m) \in \Upsilon^1$. The optimal solution of $g(\boldsymbol{h}, \boldsymbol{\xi}^k)$, say $\boldsymbol{y}^1$, satisfies $\boldsymbol{c}^\top \boldsymbol{y}^1 \leq m, \boldsymbol{A}\boldsymbol{y}^1 \geq \boldsymbol{h}, \boldsymbol{D}\boldsymbol{y}^1 \geq \boldsymbol{f}$, proving that $(\boldsymbol{h}, m) \in \Upsilon^2$. For the other direction of the proof, consider any $(\boldsymbol{h}, m) \in \Upsilon^2$. Then, there exists a vector $\boldsymbol{y}^2$ such that it satisfies $\boldsymbol{c}^\top \boldsymbol{y}^2 \leq m, \boldsymbol{A}\boldsymbol{y}^2 \geq \boldsymbol{h}, \boldsymbol{D}\boldsymbol{y}^2 \geq \boldsymbol{f}$. As $\boldsymbol{y}^2$ is a feasible solution of the problem $\min_{\boldsymbol{y}}\{\boldsymbol{c}^\top \boldsymbol{y} : \boldsymbol{A}\boldsymbol{y} \geq \boldsymbol{h}, \boldsymbol{D}\boldsymbol{y} \geq \boldsymbol{f}\}$, $g(\boldsymbol{h}, \boldsymbol{\xi}^k) \leq \boldsymbol{c}^\top \boldsymbol{y}^2 \leq m$, and therefore, $(\boldsymbol{h}, m) \in \Upsilon^1$. $\square$

Combining Lemma 1 with the monolithic formulation (6), we propose a mixed-integer linear programming reformulation of Model (3) as follows.

Theorem 2. Using the ambiguity set defined in (9), Model (3) is equivalent to the following mixed-integer linear program:

$$
\begin{aligned}
\min \quad & \sum_{i \in \mathcal{I}} c_i^o x_i + \sum_{i \in \mathcal{I}, t \in \mathcal{T}} c_i^h h_{it} - \alpha_1 - \sum_{j \in \mathcal{J}, t \in \mathcal{T}} \alpha_{2jt}(\mu_{jt} - \epsilon_{jt}^\mu) - \sum_{j \in \mathcal{J}, t \in \mathcal{T}} \alpha_{3jt}(\mu_{jt}^2 + \sigma_{jt}^2)\underline{\epsilon}_{jt}^S \\
& + \beta_1 + \sum_{j \in \mathcal{J}, t \in \mathcal{T}} \beta_{2jt}(\mu_{jt} + \epsilon_{jt}^\mu) + \sum_{j \in \mathcal{J}, t \in \mathcal{T}} \beta_{3jt}(\mu_{jt}^2 + \sigma_{jt}^2)\bar{\epsilon}_{jt}^S
\end{aligned} \tag{11a}
$$

s.t. (3b)–(3d)

$$
-\alpha_1 + \beta_1 + \sum_{j \in \mathcal{J}, t \in \mathcal{T}} \xi_{jt}^k(-\alpha_{2jt} + \beta_{2jt}) + \sum_{j \in \mathcal{J}, t \in \mathcal{T}} (\xi_{jt}^k)^2(-\alpha_{3jt} + \beta_{3jt}) \geq \Phi^k, \ \forall k \in [K], \tag{11b}
$$

$$
\Phi^k = \sum_{i \in \mathcal{I}, j \in \mathcal{J}, t \in \mathcal{T}} c_{ijt}^s s_{ijt}^k + \sum_{j \in \mathcal{J}, t \in \mathcal{T}} \left(c_{jt}^I I_{jt}^k + c_{jt}^u u_{jt}^k \right), \ \forall k \in [K], \tag{11c}
$$

(4b)–(4d)

$$
\boldsymbol{\alpha}, \ \boldsymbol{\beta} \geq \boldsymbol{0}. \tag{11d}
$$

Proof. To obtain the mixed-integer linear programming reformulation, we first revise the monolithic formulation (6) under the ambiguity set defined in (9). Then, we derive a polyhedral representation of the set $\{(\boldsymbol{h}, m) : g(\boldsymbol{h}, \boldsymbol{\xi}^k) \leq m\}$ where m is the left-hand side of constraint (6b). Using Lemma 1 and the definition of the function $g(\boldsymbol{h}, \boldsymbol{\xi}^k)$, we derive the resulting formulation (11). $\square$

5 Case Studies of COVID-19 Vaccine and Test Kit Distribution

In this section, we present two comprehensive case studies of the presented optimization frameworks to conduct resource distribution under uncertain spatiotemporal demand for COVID-19 testing and vaccination. In Section 5.1, we consider COVID-19 vaccine distribution in the US, and in Section 5.2, we consider COVID-19 test kit distribution in the State of Michigan. We use Gurobi 9.0.3

coded in Python 3.6.8 for solving all mixed-integer programming models. Our numerical tests are conducted on a Windows 2012 Server with 128 GB RAM and an Intel 2.2 GHz processor.

5.1 Vaccine Distribution in the US

5.1.1 Experimental design and setup

First, we consider different vaccine allocation phases following the government and CDC's guidelines, where in the earlier phases only healthcare workers and prioritized population groups (e.g., seniors more than 65 years old) are targeted for vaccination and in the later phases, larger segments of the population are recommended for vaccination to stop virus transmission. Specifically, we follow a recent epidemiological study by Wang et al. (2020) and consider three phases to distribute the vaccines, aiming to vaccinate 6.18%, 41.97%, 51.85% of the overall adult population in the US, respectively. We also take into account certain levels of vaccine hesitancy in the population during each phase, and follow the results by Malik et al. (2020) who surveyed the US adult population to understand the acceptance of COVID-19 vaccines, among 10 Department of Health and Human Services (DHHS) regions listed below. (We exclude remote islands from these regions and only focus on the mainland US, Alaska, Hawaii and Puerto Rico.)

- Region 1 – Boston (Connecticut, Maine, Massachusetts, New Hampshire, Rhode Island, and Vermont);

- Region 2 – New York (New Jersey, New York, and Puerto Rico);

- Region 3 – Philadelphia (Delaware, District of Columbia, Maryland, Pennsylvania, Virginia, and West Virginia);

- Region 4 – Atlanta (Alabama, Florida, Georgia, Kentucky, Mississippi, North Carolina, South Carolina, and Tennessee);

- Region 5 – Chicago (Illinois, Indiana, Michigan, Minnesota, Ohio, and Wisconsin);

- Region 6 – Dallas (Arkansas, Louisiana, New Mexico, Oklahoma, and Texas);

- Region 7 – Kansas City (Iowa, Kansas, Missouri, and Nebraska);

- Region 8 – Denver (Colorado, Montana, North Dakota, South Dakota, Utah, and Wyoming);

- Region 9 – San Francisco (Arizona, California, Hawaii, Nevada);

- Region 10 – Seattle (Alaska, Idaho, Oregon, and Washington).

We select the representative cities in the DHHS regions as our demand sites and obtain the adult population in each region from the US Census Data. Based on the acceptance rate estimates and sample sizes of the surveys conducted by Malik et al. (2020), we compute a 90% confidence interval of the acceptance rate for each region, depicted in Table 1. We then multiply these values by the

total adult population in each region to obtain lower and upper bounds on the number of people to be vaccinated. As each person needs to get two doses of vaccines, we multiply these bounds by 2 to determine the number of doses needed (i.e., potential demand). To represent the demand uncertainty, we sample scenarios following uniform distributions between the demand lower and upper bounds. Table 2 summarizes the mean values of the estimated demand during the three phases for each DHHS region.

Table 1: Confidence intervals of COVID-19 vaccines' acceptance rates in 10 DHHS regions

Regions	Region 1	Region 2	Region 3	Region 4	Region 5	Region 6	Region 7	Region 8	Region 9	Region 10
Acceptance	68.06%	43.14%	72.04%	59.76%	39.13%	74.42%	72.22%	80.00%	67.61%	70.00%
90% CI LB	59.02%	31.73%	64.39%	50.85%	22.39%	68.95%	54.86%	65.29%	58.47%	60.99%
90% CI UB	77.09%	54.55%	79.70%	68.66%	55.87%	79.89%	89.59%	94.71%	76.74%	79.01%

Table 2: Estimated demand mean values during the three phases in 10 DHHS regions

Regions	Region 1	Region 2	Region 3	Region 4	Region 5	Region 6	Region 7	Region 8	Region 9	Region 10	Total
Phase 1	1.0M	1.3M	2.2M	3.9M	2.0M	3.0M	970.0K	920.4K	3.3M	968.5K	19.4M
Phase 2	6.8M	9.0M	14.7M	26.3M	13.4M	20.1M	6.6M	6.3M	22.6M	6.6M	132.4M
Phase 3	8.4M	11.2M	18.2M	32.5M	16.6M	24.8M	8.1M	7.7M	27.9M	8.1M	163.5M
Total	16M	22M	35M	63M	32M	48M	16M	15M	54M	16M	316M

As the sizes of populations to be vaccinated vary during different phases, we assume the lengths of the three phases to be 1, 2, and 3 months, respectively, with one period in our models being 2 weeks, and the demand of each phase is evenly distributed for each period. To determine candidate locations for siting DCs, we first consider the ones being used for vaccine production in the US currently. There are 5 DCs used by Pfizer-BioNTech and Moderna in the US. As these facilities are already available, we set their corresponding $\boldsymbol{x}$-values as 1 in all the models. We select representative cities of the 10 DHHS regions as potential locations to open additional DCs, and Table 3 depicts all the 15 DC locations and 10 demand locations. For each DC $i \in \mathcal{I}$, we calculate the capacity upper bound M_i by assuming the daily maximum production to be 500,000, 750,000 and 1,000,000 doses for Phases 1, 2 and 3, respectively, as manufacturers will raise their daily production capacity as the demand increases. For each $t \in \mathcal{T}$, the temporal capacity of manufacturing vaccines B_t is set as the sum of the maximum capacities over all DCs. We also examine the case when the supply chain of vaccines experiences certain disruptions and set the corresponding temporal capacities B_t as 10% of the normal values. The operating cost c_i^o for each DC $i \in \mathcal{I}$ is estimated as 10000 times the local unit warehouse rental price per square foot, by assuming a standard warehouse is about 10000 square feet. The unit capacity cost c_i^h is set as \$25 for each $i \in \mathcal{I}$, which is the average market price of one dose of COVID-19 vaccine. The unit inventory cost c_{jt}^I is estimated as the sum of low-temperature inventory cost and energy cost of common refrigerators for storing vaccines, which is \$0.00008 for each $j \in \mathcal{J}$, $t \in \mathcal{T}$. The unit shipping cost c_{ijt}^s for each region $j \in \mathcal{J}$ and supplier $i \in \mathcal{I}$ consists of two parts: The first part is the shipping cost for trucks calculated as \$3 per mile times the distance traveled from i to j in miles divided by 230,400, following the fact that each truck on average can carry 230,400 doses of Moderna vaccines (Moderna, Inc., 2021), and the second part is the refrigerated trucks' overall cost per liter of vaccine transported (PATH, World

Health Organization (WHO), 2013). The penalty cost c_{jt}^u of each unit of unsatisfied demand is set to $100 and is varied later for sensitivity analysis.

Table 3: Locations of 10 customers sites, 15 candidate DCs and optimal solutions for Phase 1 given by Deterministic (DT), Stochastic (SP) and Distributionally Robust Optimization (DRO) approaches

City	Customer sites	Candidate DCs	DT	SP	DRO
Kalamazoo, MI		already opened			
Pleasant Prairie, WI		already opened		✓	
Bloomington, IN		already opened			✓
Norwood, MA		already opened	✓	✓	✓
Saint Louis, MO		already opened		✓	
Boston	✓	candidate			
New York City, NY	✓	candidate	✓	✓	
Philadelphia, PA	✓	candidate	✓		✓
Atlanta, GA	✓	candidate	✓	✓	✓
Chicago, IL	✓	candidate	✓		✓
Dallas, TX	✓	candidate	✓	✓	✓
Kansas City, KS	✓	candidate	✓		✓
Denver, CO	✓	candidate	✓		✓
San Francisco, CA	✓	candidate	✓	✓	
Seattle, WA	✓	candidate	✓		✓

5.1.2   Results

We compute optimal solutions using three different approaches ("DT" for Deterministic, "SP" for Stochastic Programming and "DRO" for Distributionally Robust Optimization) based on 100 in-sample scenarios and then evaluate them in 1000 out-of-sample scenarios, both of which are generated independently from the same uniform distribution between the demand lower and upper bounds. For DT, we simply replace the uncertain demand with mean values shown in Table 2. For DRO, the discrete support consists of the 100 in-sample scenarios, and we set $\epsilon_{jt}^\mu = 0.5\mu_{jt}$, $\underline{\epsilon}_{jt}^S = 0.1$, $\bar{\epsilon}_{jt}^S = 2$ for all $j \in \mathcal{J}$, $t \in \mathcal{T}$. For each approach, we display the DCs that are open and actively ship out vaccines in the optimal solutions of Phase 1's problem in Table 3.

To summarize the out-of-sample performance of optimal solutions given by the three approaches, we provide Table 4, where we rank the models from the most preferred (= 1) to the least preferred (= 3) in terms of the resultant amounts of unsatisfied demand and overall cost, respectively. The DRO approach cannot solve the problem to optimality or even obtain feasible solutions within the computational time limit (being 2 hours) for Phases 2 and 3. As a result, we only compare DT and SP for these two phases.

From Table 4, in Phase 1, DRO obtains the least amount of unsatisfied demand and the second highest cost overall, while DT performs the worst in terms of both demand satisfaction and overall cost. When facing scarce resources (i.e., 10% of the regular capacities), the ranking remains the same in Phase 1 because all three approaches do not use up all the resources. However, when

14

Table 4: Out-of-sample performance of different approaches in terms of unmet demand and overall cost for Phases 1, 2, 3 of vaccine distribution in the US.

Phases	Model	Unsatisfied Demand		Overall Costs	
		Ample	Scarce	Ample	Scarce
Phase 1	DT	3	3	3	3
	SP	2	2	1	1
	DRO	1	1	2	2
Phase 2	DT	2	1	2	1
	SP	1	1	1	1
	DRO	-	-	-	-
Phase 3	DT	2	1	2	2
	SP	1	1	1	1
	DRO	-	-	-	-

the resource capacity becomes tight such as in Phases 2 and 3, the results are almost identical for different models as there is not much flexibility in making different production and shipment plans. In terms of the overall cost, SP always outperforms the other two approaches. We note that the raw cost breakdowns of each approach are detailed in Tables 8 and 9 in the Appendix. Next, we focus on the analysis of optimal solutions of different methods under the setting of ample resources.

The average shipments in the optimal solutions of SP and DRO for Phase 1's vaccine distribution are presented in Figures 1 and 2, respectively. From Figure 1, seven DCs are selected in the optimal solution, and among them four are the representative cities in regions with high demand volumes, and three are from the existing Pfizer-BioNTech and Moderna open DCs. On the other hand, the other two existing DCs do not produce or ship any vaccines either because they are too close to some other open DCs in the optimal solution or they reside in the areas having low demand volumes. Moreover, the top five largest shipments are from DCs to their nearest demand sites (i.e., New York City to Philadelphia, Pleasant Prairie to Chicago, Saint Louis to Kansas City, Dallas to Denver, and San Francisco to Seattle), and each requires up to five trucks if fully occupied and the delivery time will be all within two days. All the other longer-distance shipments are in smaller volumes, requiring only one truck. For example, the longest-distance shipment is from Norwood to Seattle, which may take 4 to 5 days according to UPS's estimation, but it only carries 25 doses of vaccines. Comparing Figure 2 with Figure 1, DRO selects more DCs to open, among them only two are existing open ones. The number of shipment routes also increases significantly. As San Francisco is not an open DC anymore, the largest shipment occurs between Seattle and San Francisco and requires 8 trucks and 2 days to transit. The second and third largest shipments are from Philadelphia to New York City and Norwood to Boston, respectively, both requiring 3 trucks and 1 day.

Furthermore, we present Phase 1's unsatisfied demand mean, standard deviation, and 75 to 95 percentile values in the 1000 out-of-sample scenarios according to the three approaches in Figure 3a, and average unsatisfied demand percentages in each region in Figure 3b, respectively. From Figure 3, DRO attains the least amount of unsatisfied demand while DT performs the worst. Comparing
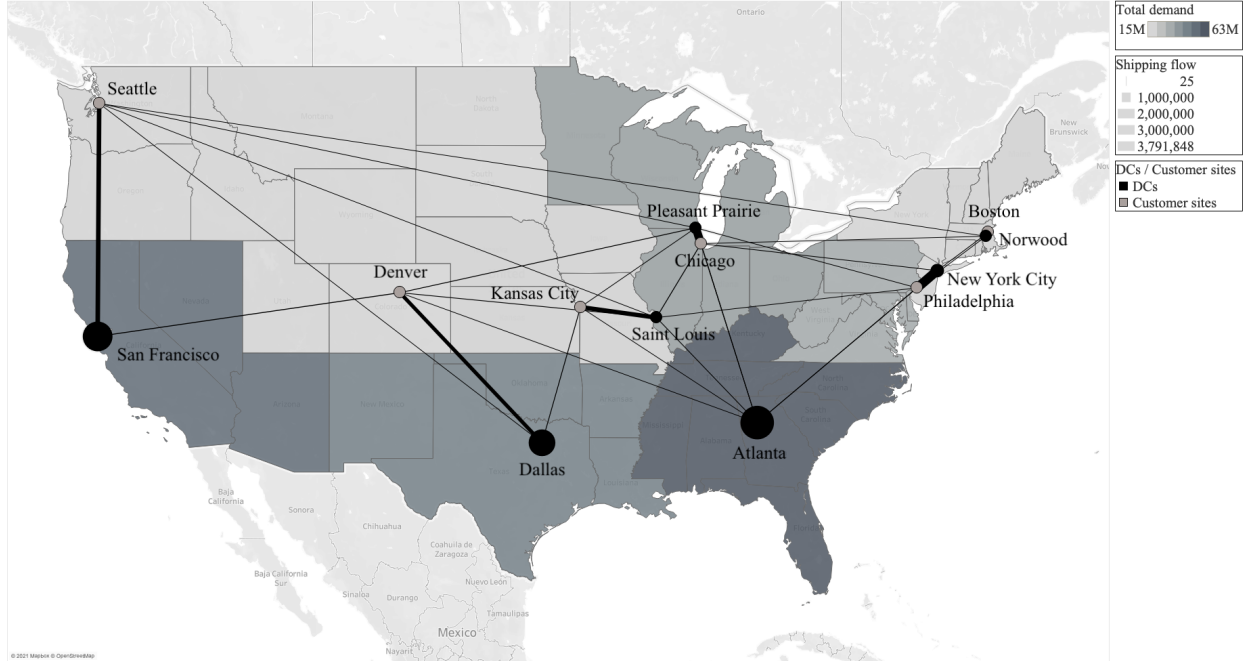
Figure 1: Average shipments of Phase 1's vaccines in 1000 out-of-sample scenarios given by the optimal solution of the SP approach. The background color of 10 DHHS regions indicates the total demand across all three phases where darker color represents higher demand volume. The black and gray circles stand for open DCs and demand sites, respectively, while DCs located in New York City, Atlanta, Dallas and San Francisco are also demand sites themselves and the sizes of these black circles represent the amount of vaccines they produce for satisfying their own demand. The black lines represent shipments from open DCs to demand locations with wider lines meaning higher volumes.

the results in different regions, Region 5 – Chicago does not meet over 4% of the demand in DT approach, and Region 8 – Denver does not cover about 4% of the demand in SP approach, both of which have relatively low demand volumes according to Table 2.

Lastly, we compare the vaccine allocation results in the SP approach with the current Pfizer-BioNTech and Moderna's status reported by CDC (Center for Disease Control and Prevention, 2021b,a). From CDC's website, Pfizer-BioNTech has started to provide first-dose vaccines since December 14, 2020, with the same amount of second-dose vaccines arriving three weeks later, while Moderna started to ship first-dose vaccines on December 21, 2020, with a four-week delay in the second-dose shipments. Consequently, we let December 14, 2020 be the starting date of Phase 1 and denote Phase 1-1 as the first two-week period of Phase 1 (i.e., December 14, 2020 – December 28, 2020). We report the total number of doses that our SP approach and CDC have allocated in each period in Table 5, and display the number of doses each region has received in each period in Figure 4 as of February 8, 2021.

From Table 5 and Figure 4, CDC almost doubled the vaccine allocations in Phase 1; however, it falls behind in Phase 2 and as of February 8, 2021, the total amount of vaccines distributed by Pfizer-BioNTech and Moderna does not reach the benchmark given by SP approach. Moreover, it
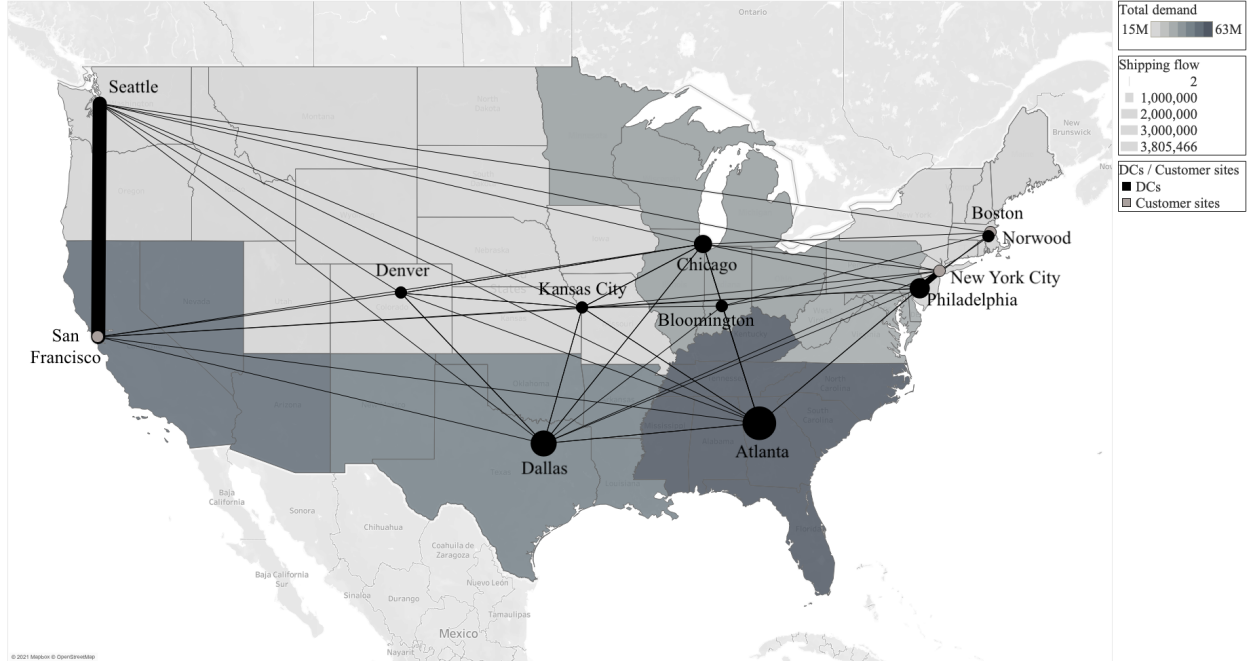
Figure 2: Average shipments of Phase 1's vaccines in 1000 out-of-sample scenarios given by the optimal solutions of the DRO approach. The background color of 10 DHHS regions indicates the total demand across all three phases where darker color represents higher demand volume. The black and gray circles stand for open DCs and customer sites, respectively, while DCs located in Philadelphia, Chicago, Atlanta, Dallas, Kansas City, Denver and Seattle are also demand sites themselves and the size of these black circles represent the amount of vaccines they produced for satisfying their own demand. The black lines represent shipments from open DCs to demand locations with wider lines meaning higher volumes.

Table 5: Total number of doses in the optimal solutions of SP and CDC's reported data for each period as of February 8, 2021

Approaches	Phases 1-1 & 1-2	Phases 2-1 & 2-2	Total
SP	19M	71M	90M
CDC	38M	34M	72M

is worth noting that when calculating the vaccines distributed by Pfizer-BioNTech and Moderna, we assume that the first-dose and second-dose shipments will be received three weeks apart by ignoring the transportation delay. As a result, the number reported in the "CDC" row of Table 5 will be slightly higher than the real-time data tracker such as Center for Disease Control and Prevention (2021c) .

5.2   COVID-19 Test Kit Allocation in Michigan, USA

5.2.1   Experimental Design and Setup

To demonstrate that the presented generic optimization approaches are well-suited for various resources over different scale problems, we focus on the COVID-19 test kit resource allocation

17

(a) Unsatisfied demand statistics

(b) Regional unsatisfied demand
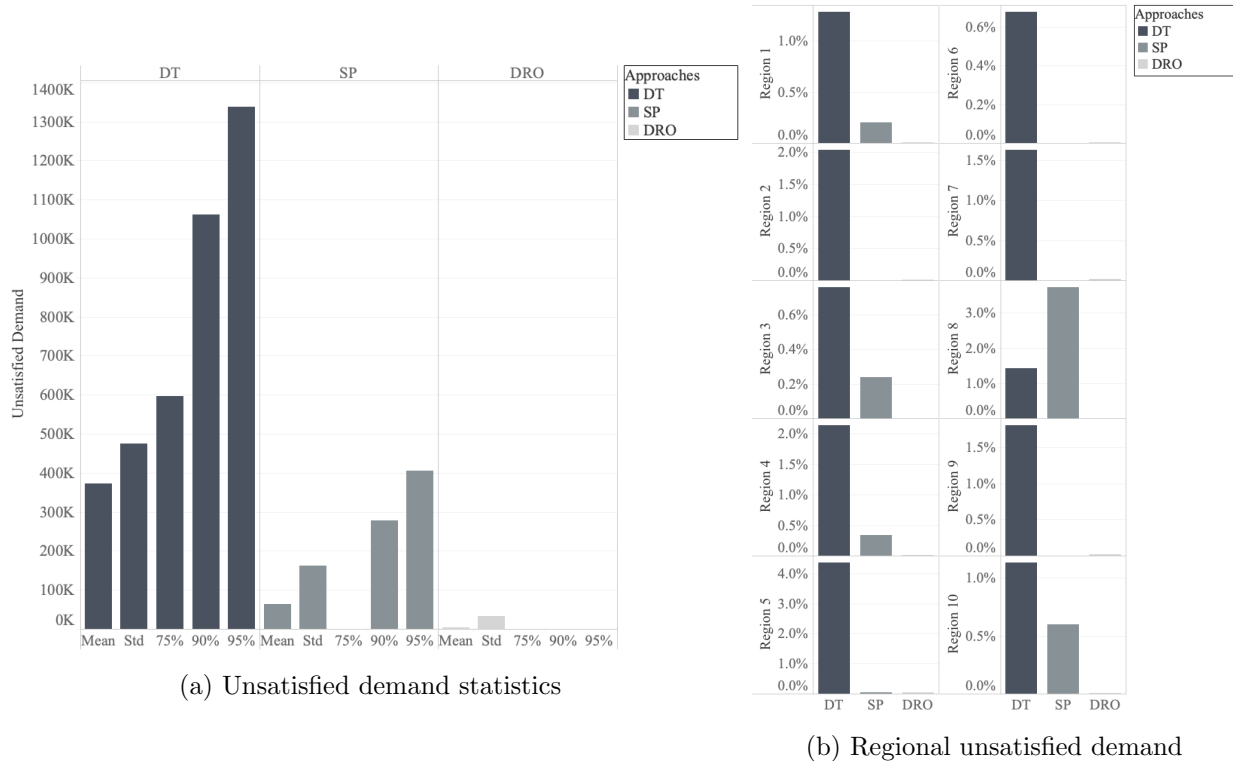
Figure 3: Unsatisfied demand given by vaccine distribution in Phase 1 of different approaches.

problem in Michigan, and divide the state into eight emergency preparedness regions according to Figure 5. For ensuring distribution of these resources, we consider these regions as representatives of demand locations. Note that Regions 2N, 2S, 3 are renamed as Regions 2, 3 and 4 for notation simplicity in the case study. We pick 29 suppliers in Michigan as the candidate locations of the distributions centers.

For predicting demand and generating uncertain scenarios, we mainly follow Pei and Shaman (2020), which projects the daily new confirmed cases in the US at county level based on a meta-population Susceptible-Exposed-Infectious-Removed (SEIR) model. The projections are reported in the 2.5, 25, 50, 75, 97.5 percentiles for each county and day, and regularly updated to capture different trends in virus transmission and intervention policies over the pandemic. To identify the demand of each emergency preparedness region, we first calculate the percentiles of the total projected confirmed cases, and then divide them by our targeted positivity rate (i.e., 5%), meaning that we aim to test 100 persons if there are 5 confirmed cases. Having obtained the percentiles of the projected demand, we extract the mean and variance according to Wan et al. (2014) by assuming the 2.5 and 97.5 percentile values being lower and upper bounds of the support of the underlying random demand for estimation.

We consider different planning horizons to represent various phases of virus transmission. The trend of the disease transmission in Michigan is depicted in Figure 6. From Figure 6, the number of infected cases reached the first peak in April, 2020. It was then controlled in June, 2020 with the
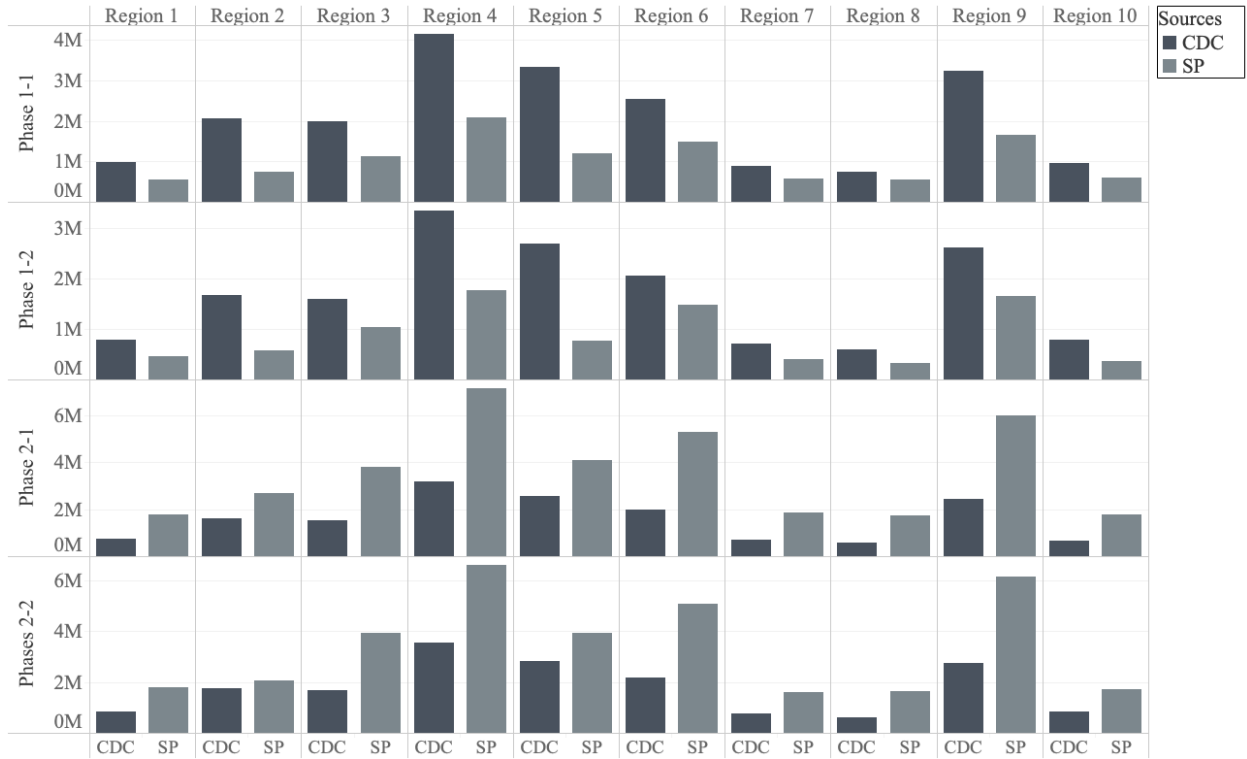
Figure 4: Comparison of the number of doses each region received in different periods between CDC's reported data and our SP approach.
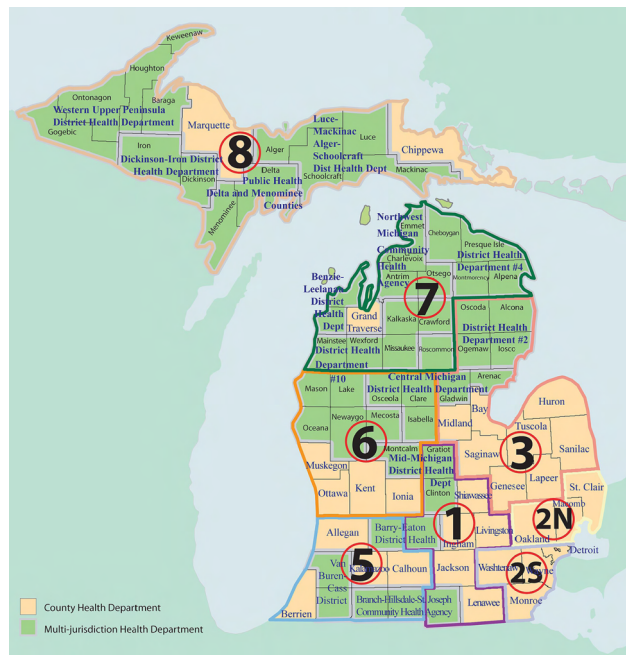
Figure 5: Michigan Emergency Preparedness Regions (source: Michigan state government).

regulations from governor's executive orders and closures of businesses and public services. Around December, winter holiday gatherings increased virus spread, and thus resulted in another peak and

continued transmissions. Consequently, we select April 5, June 4 and December 20 as the starting dates of the planning horizon, where we consider a two-week planning horizon with one period being one week. As a result, we examine the presented approaches over (i) peak periods (i.e., April 5 – April 19), (ii) off-peak periods where we can still observe the effects of closures (i.e., June 4 – June 18), and (iii) continued transmission case (i.e., December 20 – January 3).

Cases by Date of Onset
Case Status ●Confirmed ●Probable
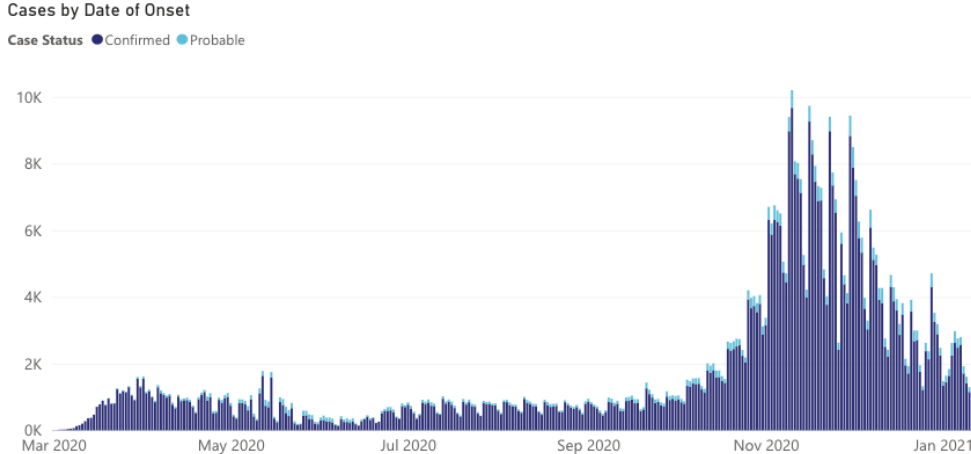
Figure 6: The number of infectious cases by date of onset in Michigan between March 2020 and January 2021.

In terms of parameter choices, we set the upper bound M_i of the capacity h_{it} to the maximum production amount of supplier $i \in \mathcal{I}$ at period $t \in \mathcal{T}$ depending on the size of each supplier, and the temporal capacity of manufacturing test kits B_t to the sum of maximum capacity over all DCs for all $t \in \mathcal{T}$. We also test the case where there are only scarce resources available (usually in earlier phases of the pandemic), and set the capacity B_t to 10% of the regular capacities for all $t \in \mathcal{T}$. The operating cost c_i^o for each supplier $i \in \mathcal{I}$ is set similar to the one in the vaccine distribution case. We set the unit capacity cost c_i^h to \$20 for all $i \in \mathcal{I}$, and the unit inventory cost c_{jt}^I to the average pallet storage cost divided by the number of test kits a pallet can store for all $j \in \mathcal{J}$, $t \in \mathcal{T}$. The unit shipping costs c_{ijt}^s for all region $j \in \mathcal{J}$ and supplier $i \in \mathcal{I}$ are calculated as \$3 per mile times the distance in miles divided by the number of test kits a truck can carry. In the state-level test kit allocation problem, we examine three cases of the unit penalty c_{jt}^u for unmet demand such that we can prioritize population groups or regions during different time periods. In particular, in Case (i), we set c_{jt}^u to a constant, i.e., $c_{jt}^u = 100$ for all j and t; in Case (ii), we let c_{jt}^u be linearly dependent on the projected demand median for region j at period t, i.e., $c_{jt}^u = d_{jt}^{\mathrm{median}} + 10$ (we add a small constant to the median as some regions' demand medians are 0 in early phases but we also want to penalize the lost demand there); and in Case (iii), we set $c_{jt}^u = 0.001 d_j^{\mathrm{elder}}$ with d_{jt}^{elder} being the number of people above 65 years old in region j. In the latter two cases, we prioritize regions with more infections and more elderly or high-risk population groups, respectively.

To compare the severity of disease transmission in different regions and phases, we display the weekly projected demand median d_{jt}^{median} for 8 regions in Michigan during the three phases as well as 65 or older populations in each region in Table 6. As can be seen from Table 6, Regions 7 and 8

20

Table 6: Projected demand median during different phases and population above 65 for 8 regions

Starting date	Region 1	Region 2	Region 3	Region 4	Region 5	Region 6	Region 7	Region 8
April 5	153	3.6K	2.2K	107	2	407	31	0
June 4	43	236	516	61	112	443	0	0
December 20	55.5K	100.0K	93.3K	72.7K	52.1K	76.5K	18.8K	12.7K
Population above 65	181.8K	360.2K	349.2K	216.9K	143.5K	237.2K	84.2K	66.5K

have significantly fewer number of new cases each day and senior populations than other regions, while Regions 2 and 3 have the highest projected demand and senior population and thus will be most prioritized when we follow the penalty cost cases (ii) and (iii).

5.2.2 Results

We first obtain optimal solutions of the three models (DT, SP, DRO) based on 100 in-sample scenarios and 1000 out-of-sample scenarios following the same normal distribution with the estimated mean and variance. For DRO, we set the scaling parameters as $\epsilon_{jt}^{\mu} = 0.5\mu_{jt}$, $\underline{\epsilon}_{jt}^{S} = 0.1$, $\bar{\epsilon}_{jt}^{S} = 2$ for all $j \in \mathcal{J}$, $t \in \mathcal{T}$ in June and December and set $\epsilon_{jt}^{\mu} = \mu_{jt}$, $\underline{\epsilon}_{jt}^{S} = 0.01$, $\bar{\epsilon}_{jt}^{S} = 10$ for all $j \in \mathcal{J}$, $t \in \mathcal{T}$ in April. By fixing the penalty parameter c_{jt}^{u} to $0.001 d_j^{\text{elder}}$ for each region $j \in \mathcal{J}$ (i.e., Case (iii) penalty setting), we summarize out-of-sample performance given by solutions of the three approaches under different resource settings in Table 7, where we rank the approaches from the most preferred (= 1) to the least preferred (= 3) in terms of unsatisfied demand and overall cost, respectively. We note that the raw cost breakdowns of each approach are presented in Tables 10 and 11 in the Appendix.

Table 7: Out-of-sample performance of different approaches in the COVID-19 test kit distribution example

Phases	Model	Unsatisfied Demand		Overall Cost	
		Ample	Scarce	Ample	Scarce
	DT	3	3	3	3
April	SP	2	2	1	1
	DRO	1	1	2	2
	DT	3	3	3	3
June	SP	2	2	1	1
	DRO	1	1	2	2
	DT	3	1	3	1
December	SP	2	1	1	2
	DRO	1	1	2	3

From Table 7, in the ample resource case, DRO always obtains the least amount of unsatisfied demand, while DT performs the worst. When there are only scarce resources (i.e., 10% available), the ranking remains the same in April and June because all three models do not use up to 10% of the total resources. However, when the resource capacity becomes tight such as in December, the results of the three models are identical as there is not much flexibility in producing and shipping

test kits. In terms of overall cost, SP outperforms the other two models in most of the settings.

We display the detailed unsatisfied demand percentages in each region under different cases of penalty cost patterns in Figure 7. Comparing Figure 7 with Table 6, for Cases (ii) and (iii) penalty settings, the demand in Regions 2, 3, 4 and 6 is all satisfied, as these regions have more projected demand in December and more senior populations. On the other hand, Regions 7 and 8 always have the highest unsatisfied demand as they are farther away from the DCs and have less projected demand.
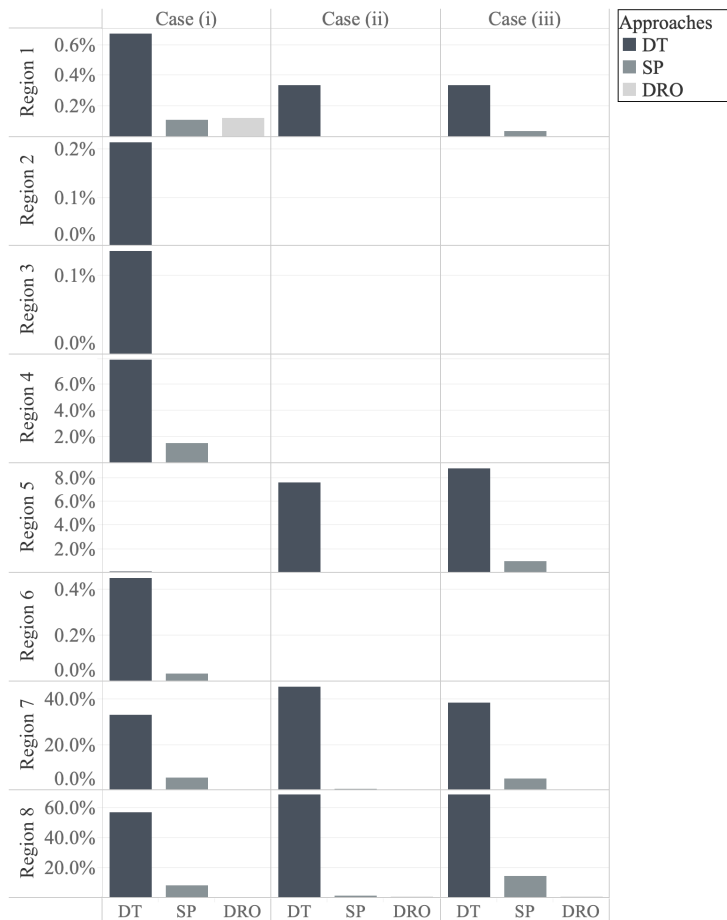
Figure 7: Unsatisfied demand percentages in each region in December with ample resources given Cases (i), (ii), (iii) unit penalty.

Next, we present the cost breakdown over different phases in Figure 8. From Figure 8, under ample resources, DRO can satisfy almost all the demand, while DT still leaves thousands of people untested. However, when we limit the resources to be 10% of the regular amounts (see gray dashed line in Figure 8), all capacity costs that exceed the gray line will be truncated to the one that uses only 10% of the original B_t. For scenarios where all approaches' capacity costs exceed 10% (e.g., December under ample resources), under scarce resources, these approaches' performance will be identical as they are limited by the total capacity, confirming the results in Table 7.
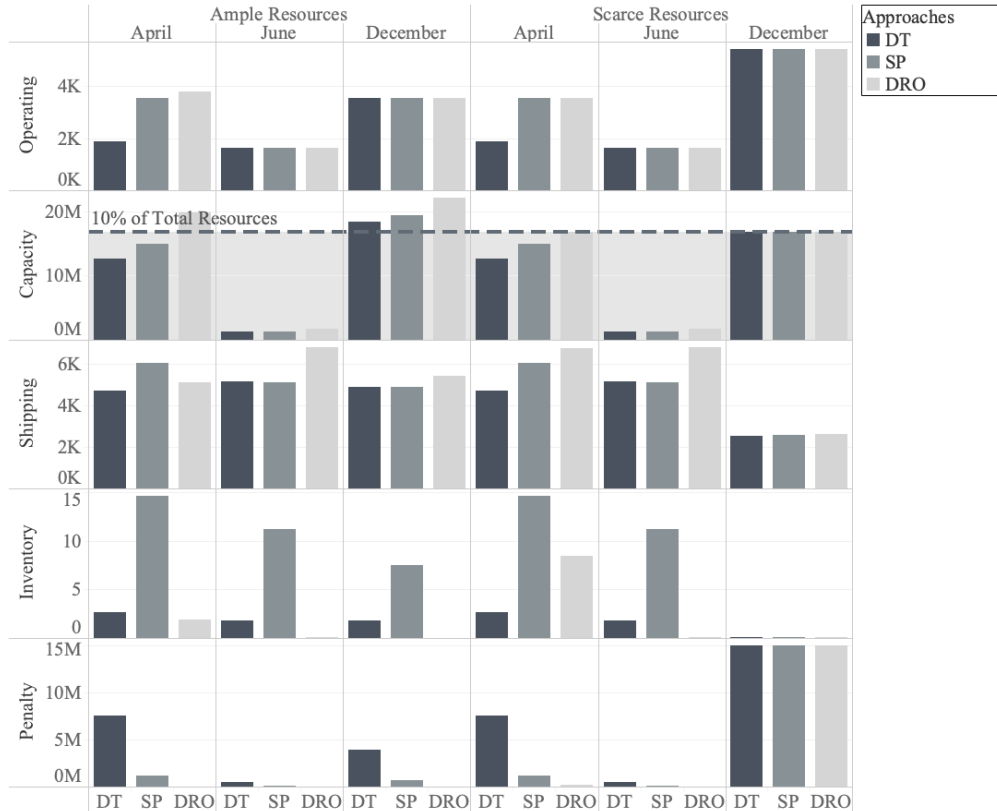
Figure 8: Cost breakdown of test kit distribution over different phases under ample resources (in dollars).

6 Conclusion

In this paper, we presented a generic framework to model resource distribution for epidemic control under spatiotemporal demand uncertainties for these resources. Depending on the level of statistical information available for characterizing the uncertainties, which are impacted by various factors including infection trends and demographic behavior, we proposed a stochastic programming and a distributionally robust optimization approach to optimize the locations and capacities of DCs along with deciding shipments to and inventory at demand sites while penalizing the unmet demand. As the proposed optimization frameworks can be applied to different scales of resource distribution, we presented two case studies using COVID-19 vaccine distribution in the US and the analogous test kit distribution in the State of Michigan. These case studies benefit from not only the existing infrastructure of the current manufacturers but also the potential DCs that can be built to facilitate the distribution of these resources. Furthermore, we considered different phases of the pandemic, ample or scarce resources, and three cases of unmet demand penalty settings to compare the results of deterministic, stochastic and robust optimization approaches.

Our approaches aim efficient and fair distribution of resources by allowing prioritization of regions with more vulnerable population groups or with higher infection susceptibility. The case studies demonstrated the importance of incorporating demand uncertainty in these planning prob-

lems as the stochastic programming and distributionally robust optimization approaches outperform the deterministic one in terms of cost and demand coverage. The distributionally robust approach provided a better worst-case performance in terms of unvaccinated or untested people who qualify, with an overall cost higher than the one of the stochastic programming approach. As the stochastic programming approach can provide an intermediate solution while considering uncertainty, its performance was compared against CDC's current distribution status of COVID-19 vaccines, demonstrating more vaccines need to be distributed across the country in the later phases for satisfying the demand and establishing the herd immunity. Furthermore, the case study of test kit distribution demonstrated the prioritization of resource allocation depending on the infection trend and vulnerable population percentages over the studied regions.

Acknowledgement

References

Babus, A., Das, S., and Lee, S. (2020). The optimal allocation of covid-19 vaccines. *medRxiv*.

Basciftci, B., Ahmed, S., and Shen, S. (2020). Distributionally robust facility location problem under decision-dependent stochastic demand. *European Journal of Operational Research*.

Bertsimas, D., Boussioux, L., Wright, R. C., Delarue, A., Digalakis, V., Jacquillat, A., Kitane, D. L., Lukin, G., Li, M. L., Mingardi, L., Nohadani, O., Orfanoudaki, A., Papalexopoulos, T., Paskov, I., Pauphilet, J., Lami, O. S., Stellato, B., Bouardi, H. T., Carballo, K. V., Wiberg, H., and Zeng, C. (2021a). From predictions to prescriptions: A data-driven response to covid-19. *Health Care Management Science*.

Bertsimas, D., Digalakis Jr, V., Jacquillat, A., Li, M. L., and Previero, A. (2021b). Where to locate covid-19 mass vaccination facilities? *arXiv preprint arXiv:2102.07309*.

Bertsimas, D., Ivanhoe, J. K., Jacquillat, A., Li, M. L., Previero, A., Lami, O. S., and Bouardi, H. T. (2020). Optimizing vaccine allocation to combat the covid-19 pandemic. *medRxiv*.

Billingham, S., Widrick, R., Edwards, N. J., and Klaus, S. A. (2020). Covid-19 (sars-cov-2) ventilator resource management using a network optimization model and predictive system demand. *medRxiv*.

Blanco, V., Gázquez, R., and Leal, M. (2020). Reallocating and sharing health equipments in sanitary emergency situations: The covid-19 case in spain. *arXiv preprint arXiv:2012.02062*.

Bubar, K. M., Kissler, S. M., Lipsitch, M., Cobey, S., Grad, Y., and Larremore, D. B. (2020). Model-informed covid-19 vaccine prioritization strategies by age and serostatus. *medRxiv*.

Cao, H. and Huang, S. (2012). Principles of scarce medical resource allocation in natural disaster relief: a simulation approach. *Medical Decision Making*, 32(3):470–476.

CDC (2020). `https://www.cdc.gov/coronavirus/2019-ncov/cases-updates/testing-in-us.html`.

Center for Disease Control and Prevention (2021a). COVID-19 Vaccine Distribution Allocations by Jurisdiction - Moderna. `https://data.cdc.gov/Vaccinations/COVID-19-Vaccine-Distribution-Allocations-by-Juris/b7pe-5nws`.

Center for Disease Control and Prevention (2021b). COVID-19 Vaccine Distribution Allocations by Jurisdiction - Pfizer. `https://data.cdc.gov/Vaccinations/COVID-19-Vaccine-Distribution-Allocations-by-Juris/saz5-9hgg`.

Center for Disease Control and Prevention (2021c). COVID Data Tracker: COVID-19 Vaccinations in the United States. `https://covid.cdc.gov/covid-data-tracker/#vaccinations`.

Chen, X., Li, M., Simchi-Levi, D., and Zhao, T. (2020). Allocation of covid-19 vaccines under limited supply. *Available at SSRN: http://dx.doi.org/10.2139/ssrn.3678986*.

Chick, S. E., Mamani, H., and Simchi-Levi, D. (2008). Supply chain coordination and influenza vaccination. *Operations Research*, 56(6):1493–1506.

Daskin, M. S. (2011). *Network and discrete location: Models, algorithms, and applications.* John Wiley & Sons.

Delage, E. and Ye, Y. (2010). Distributionally robust optimization under moment uncertainty with application to data-driven problems. *Operations Research*, 58(3):595–612.

Duijzer, L. E., van Jaarsveld, W., and Dekker, R. (2018). Literature review: The vaccine supply chain. *European Journal of Operational Research*, 268(1):174–192.

Emanuel, E. J., Persad, G., Upshur, R., Thome, B., Parker, M., Glickman, A., Zhang, C., Boyle, C., Smith, M., and Phillips, J. P. (2020). Fair allocation of scarce medical resources in the time of covid-19. *New England Journal of Medicine*, 382(21):2049–2055.

Golan, M. S., Trump, B. D., Cegan, J. C., and Linkov, I. (2020). The vaccine supply chain: A call for resilience analytics to support covid-19 vaccine production and distribution. *arXiv preprint arXiv:2011.14231*.

Gong, Q. and Batta, R. (2007). Allocation and reallocation of ambulances to casualty clusters in a disaster relief operation. *IIE Transactions*, 39(1):27–39.

Gupta, S., Starr, M. K., Farahani, R. Z., and Matinrad, N. (2016). Disaster management from a pom perspective: Mapping a new domain. *Production and Operations Management*, 25(10):1611–1637.

Huang, H.-C., Singh, B., Morton, D., Johnson, G., Clements, B., and Meyers, L. (2017). Equalizing access to pandemic influenza vaccines through optimal allocation to public health distribution points. *PLoS ONE*, 12(8):e0182720.

Jacobson, S. H., Sewell, E. C., and Proano, R. A. (2006). An analysis of the pediatric vaccine supply shortage problem. *Health Care Management Science*, 9(4):371–389.

Jiang, R. and Guan, Y. (2016). Data-driven chance constrained stochastic program. *Mathematical Programming*, 158(1):291–327.

Kleywegt, A. J., Shapiro, A., and Homem-de Mello, T. (2002). The sample average approximation method for stochastic discrete optimization. *SIAM Journal on Optimization*, 12(2):479–502.

Lampariello, L. and Sagratella, S. (2021). Effectively managing diagnostic tests to monitor the covid-19 outbreak in italy. *Operations Research for Health Care*, 28:100287.

Li, Z., Swann, J. L., and Keskinocak, P. (2018). Value of inventory information in allocating a limited supply of influenza vaccine during a pandemic. *PloS one*, 13(10):e0206293.

Liu, K., Li, Q., and Zhang, Z.-H. (2019). Distributionally robust optimization of an emergency medical service station location and sizing problem with joint chance constraints. *Transportation Research Part B: Methodological*, 119:79 – 101.

Long, E. F., Nohdurft, E., and Spinler, S. (2018). Spatial resource allocation for emerging epidemics: A comparison of greedy, myopic, and dynamic policies. *Manufacturing & Service Operations Management*, 20(2):181–198.

Malik, A. A., McFadden, S. M., Elharake, J., and Omer, S. B. (2020). Determinants of covid-19 vaccine acceptance in the us. *EClinicalMedicine*, 26:100495.

Medlock, J. and Galvani, A. P. (2009). Optimizing influenza vaccine distribution. *Science*, 325(5948):1705–1708.

Mehrotra, S., Rahimian, H., Barah, M., Luo, F., and Schantz, K. (2020). A model of supply-chain decisions for resource sharing with an application to ventilator allocation to combat covid-19. *Naval Research Logistics (NRL)*, 67(5):303–320.

Moderna, Inc. (2021). Storage and Handling of Moderna Vaccines. `https://www.modernatx.com/covid19vaccine-eua/providers/storage-handling`.

Mohajerin Esfahani, P. and Kuhn, D. (2018). Data-driven distributionally robust optimization using the wasserstein metric: performance guarantees and tractable reformulations. *Mathematical Programming*, 171(1):115–166.

Özaltın, O. Y., Prokopyev, O. A., Schaefer, A. J., and Roberts, M. S. (2011). Optimizing the societal benefits of the annual influenza vaccine: A stochastic programming approach. *Operations Research*, 59(5):1131–1143.

Parker, F., Sawczuk, H., Ganjkhanloo, F., Ahmadi, F., and Ghobadi, K. (2020). Optimal resource and demand redistribution for healthcare systems under stress from covid-19. *arXiv preprint arXiv:2011.03528*.

PATH, World Health Organization (WHO) (2013). Delivering Vaccines: A cost comparison of in-country vaccine transport container options. `https://path.azureedge.net/media/documents/TS_opt_in_country_transport_rpt.pdf`.

Pei, S. and Shaman, J. (2020). Initial simulation of sars-cov2 spread and intervention effects in the continental us. *MedRxiv*.

Santini, A. (2021). Optimising the assignment of swabs and reagent for pcr testing during a viral epidemic. *OMEGA*, 102:102341.

Shen, Z.-J. M., Zhan, R. L., and Zhang, J. (2011). The reliable facility location problem: Formulations, heuristics, and approximation algorithms. *INFORMS Journal on Computing*, 23(3):470–482.

Snyder, L. V. (2006). Facility location under uncertainty: A review. *IIE Transactions*, 38(7):537–554.

Tebbens, R. J. D. and Thompson, K. M. (2009). Priority shifting and the dynamics of managing eradicable infectious diseases. *Management Science*, 55(4):650–663.

Wan, X., Wang, W., Liu, J., and Tong, T. (2014). Estimating the sample mean and standard deviation from the sample size, median, range and/or interquartile range. *BMC Medical Research Methodology*, 14(1):1–13.

Wang, C. and Chen, S. (2020). A distributionally robust optimization for blood supply network considering disasters. *Transportation Research Part E: Logistics and Transportation Review*, 134:101840.

Wang, W., Wu, Q., Yang, J., Dong, K., Chen, X., Bai, X., Chen, X., Chen, Z., Viboud, C., Ajelli, M., and Yu, H. (2020). Global, regional, and national estimates of target population sizes for covid-19 vaccination: descriptive study. *BMJ*, 371.

Westerink-Duijzer, E. (2017). *Mathematical Optimization in Vaccine Allocation*.

Xiang, Y. and Zhuang, J. (2016). A medical resource allocation model for serving emergency victims with deteriorating health conditions. *Annals of Operations Research*, 236(1):177–196.

Zachary A. Collier, J. M. K., Trump, B. D., Cegan, J. C., and Sarah Wolberg, I. L. (2020). Value-based optimization of healthcare resource allocation for covid-19 hot spots. *arXiv preprint arXiv:2011.14233*.

Zhang, Y., Jiang, R., and Shen, S. (2018). Ambiguous chance-constrained binary programs under mean-covariance information. *SIAM Journal of Optimization*, 28(4):2922–2944.

Appendix: Additional results

We first present the detailed results of cost breakdown in the national vaccine allocation and state-level test kit distribution problems under different phases, resource settings and approaches.

Table 8: Cost breakdown of vaccine distribution under ample resources, different phases and approaches

Phases	Approaches	Operating	Capacity	Shipping	Inventory	Penalty	Total
	DT	$97K	$486M	$39K	$34	$37M	$524M
Phase 1	SP	$63K	$496M	$48K	$155	$6M	$503M
	DRO	$76K	$515M	$55K	$80	$292K	$516M
	DT	$194K	$3B	$143K	$202	$287M	$4B
Phase 2	SP	$175K	$3B	$117K	$1K	$29M	$3B
	DRO			N.A.			
	DT	$290K	$4B	$184K	$405	$366M	$4B
Phase 3	SP	$263K	$4B	$144K	$2K	$40M	$4B
	DRO			N.A.			

Table 9: Cost breakdown of vaccine distribution under scarce resources, different phases and approaches

Phases	Approaches	Operating	Capacity	Shipping	Inventory	Penalty	Total
	DT	$97K	$486M	$39K	$34	$37M	$524M
Phase 1	SP	$63K	$496M	$52K	$99	$7M	$503M
	DRO	$54K	$512M	$58K	$64	$687K	$513M
	DT	$105K	$2B	$49K	$0	$17B	$19B
Phase 2	SP	$105K	$2B	$49K	$0	$17B	$19B
	DRO			N.A.			
	DT	$256K	$3B	$125K	$0	$13B	$16B
Phase 3	SP	$161K	$3B	$153K	$0	$13B	$16B
	DRO			N.A.			

Table 10: Cost breakdown of test kit distribution under ample resources, different phases and approaches

Phases	Approaches	Operating	Capacity	Shipping	Inventory	Penalty	Total
	DT	$2K	$13M	$5K	$3	$8M	$20M
April	SP	$4K	$15M	$6K	$15	$1M	$16M
	DRO	$4K	$20M	$5K	$2	$1K	$20M
	DT	$2K	$1M	$5K	$2	$490K	$2M
June	SP	$2K	$1M	$5K	$11	$94K	$1M
	DRO	$2K	$2M	$7K	$0	$1K	$2M
	DT	$4K	$18M	$5K	$2	$4M	$22M
December	SP	$4K	$19M	$5K	$7	$642K	$20M
	DRO	$4K	$22M	$5K	$0	$16K	$22M

Table 11: Cost breakdown of test kit distribution under scarce resources, different phases and approaches

Phases	Approaches	Operating	Capacity	Shipping	Inventory	Penalty	Total
	DT	$2K	$13M	$5K	$3	$8M	$20M
April	SP	$4K	$15M	$6K	$15	$1M	$16M
	DRO	$4k	$17M	$8K	$8	$181K	$17M
	DT	$2K	$1M	$5K	$2	$490K	$2M
June	SP	$2K	$1M	$5K	$11	$94K	$1M
	DRO	$2K	$2M	$7K	$0	$1K	$2M
	DT	$5K	$17M	$3K	$0	$15M	$32M
December	SP	$5K	$17M	$3K	$0	$15M	$32M
	DRO	$5K	$17M	$3K	$0	$15M	$32M